Journal of Materials Chemistry A

PAPER

View Article Online
View Journal | View Issue

Cite this: J. Mater. Chem. A, 2016, 4, 2305

Amino acid mediated mesopore formation in LTA zeolites†

Zhuwen Chen,[a] Jian Zhang,[a] Bole Yu,[a] Guangchao Zheng,[a] Jing Zhao[ab] and Mei Hong*[a]

Received 3rd December 2015
Accepted 18th January 2016

DOI: 10.1039/c5ta09860b

www.rsc.org/MaterialsA

Mesoporous LTA zeolites have been hydrothermally synthesized by using amino acids as a mesoporogen. Amino acids of carnitine, lysine, or their salt derivatives were able to generate disordered mesopores of 10–20 nm within single crystalline LTA zeolites. Unlike other mesopore generating templates such as surfactants or polymers, the amino acid templates could be easily removed by washing with water, eliminating the energy-intensive calcination step. A possible crystallization process involving three-dimensional assembly of amino acid templates *via* hydrogen bonding and electrostatic interaction was proposed, as it was found that hydrogen bonding is crucial in hierarchical structure generation, and that hydroxyl group shielded acetyl carnitine yielded no mesopores. The obtained hierarchically mesoporous LTA zeolites exhibited a remarkably higher adsorption capacity (264 mg g^{-1}) for catalase enzyme, and retained greater enzyme activity (>90%) than did conventional LTA.

1. Introduction

Recent decades have seen significant progress in the development of mesoporous zeolitic materials that possess hierarchical porous architectures.[1–5] The creation of mesopores in zeolite materials is highly desirable to overcome the great diffusion limitations imposed by the inherent micropores in the size range of 0.3–1.5 nm.[6] Various methods have been developed for creating mesoporosity in zeolites, including removal of framework atoms,[7] hard templating,[8] and soft templating.[9,10] Soft templates typically include surfactants or soft polymers which have a relatively flexible structure. However, the ordinary surfactants that succeeded in the synthesis of amorphous mesoporous silica, resulted in phase separation when employed in zeolite synthesis.[11,12] The supramolecular templating mechanism of the surfactant micelles that assisted the assembly of amorphous mesoporous materials acted competitively rather than cooperatively with the molecular templating mechanism for zeolites, leading to surfactant exclusion from the aluminosilicate domain during the zeolite crystallization process. To overcome this phase-segregation problem, specially designed or exquisitely chosen soft templates including amphiphilic organosilanes,[13–18] bifunctional polyquaternary ammonium surfactants,[9,10,19] and cationic polymers,[13,20,21] have been successfully developed. Bifunctional polyquaternary ammonium surfactants usually yield a lamellar or hexagonal zeolite structure on the mesoscale, while organosilane surfactants yield aggregated nanocrystals. Zhu *et al.*[22] ascribed this lack of long-range order phenomena to the thermodynamic and kinetic incompatibility of the zeolite framework generation process and the mesopore formation pathway, and found that even specially designed surfactants still favor ordered mesostructures due to micelle formation, sacrificing the continuity of the zeolite framework. Therefore, they rationally chose cationic polymer templates with weaker interactions than surfactants to synthesize a single crystalline zeolite with disordered mesopores, which exhibited excellent hydrothermal stability. Although purified cationic polymers mediated mesopore formation in zeolite beta, small molecules such as monomers or structural units of polymers were not able to direct the structure of zeolite beta. Later on, Zhang *et al.*[23] reported that cationic center separation of the cationic polymer structure was important for hierarchical structure generation in zeolites. While a copolymer of epichlorohydrin-*N*,*N*-dimethyl-1,3-diaminopropane copolymer (PCA) templated mesoporous ZSM-5 zeolite, its structural analogue epichlorohydrin–dimethylamine polyamine (PCS) only led to bulky ZSM-5 zeolite crystals with low mesoporosity, because PCS completely decomposed under the hydrothermal synthesis conditions while the stability of PCA was improved due to the more widely separated cationic centers. On the basis of these previous observations, we hypothesize that by using small molecules that have zwitterionic structures with positive and negative charge centers widely separated, mesoporous zeolites might be achievable. The ionic small molecules would

[a]Guangdong Provincial Key Laboratory of Nano-Micro Materials Research, School of Chemical Biology & Biotechnology, Peking University Shenzhen Graduate School, Shenzhen 518055, China. E-mail: hongmei@pkusz.edu.cn

[b]Institute of Chemistry and BioMedical Sciences, State Key Laboratory of Pharmaceutical Biotechnology, School of Life Sciences, Nanjing University, Nanjing, 210093, China

† Electronic supplementary information (ESI) available: Fig. S1–S6 are included. See DOI: 10.1039/c5ta09860b

be advantageous over polymers due to their structural flexibility, high stability, and high solubility.

Inspired by the long-established biomineralization process,[24,25] as well as the conformation-specific interaction between a zeolite framework and biologically important molecules such as amino acids,[26–28] we were attracted to the question of whether these small molecules, while altering zeolite crystallization kinetics,[29–31] could mediate mesopore formation. We embarked on our study of LTA zeolites, the most hydrophilic type of zeolite with eight-membered ring apertures of 0.42 nm, and a Si/Al ratio of 1. Although extensive studies have been carried out on the synthesis of mesoporous zeolites, reports on mesoporous LTA zeolites are rare. The reason for this partly lies in the fact that hard templates like carbon nanoparticles are incompatible with the hydrothermal synthesis conditions of zeolite LTA frameworks, and it is not easy to synthesize mesoporous LTA zeolites even when a carbon aerogel is used.[32,33] A soft template like polymer may induce reversed crystal growth to form a core–shell structure with an amorphous interior.[33–37] Ingeniously designed organosilane surfactants synthesized using multiple steps were first reported by Ryoo[14] and coworkers as mesopore generating templates in order to overcome the phase separation of surfactant micelles and the growing zeolite phase by covalently bonding to an aluminosilicate structure. Then, this method was continued by Ryoo and followed by other groups to synthesize mesoporous LTA zeolites.[17,38–44] It should be noted that the mesopore size was mostly smaller than 10 nm unless a pore expansion agent such as triblock copolymer Pluronic P123 was used simultaneously.[17] The mesopore templates used in these studies tend to be expensive and were encapsulated within or covalently bonded to the growing zeolite, which needs a post-synthetic calcination step to release the mesoporosity.

In this study, we demonstrate for the first time that an amino acid can work as an inexpensive mesopore generating agent to synthesize hierarchically structured LTA zeolite single crystals with mesopores larger than 10 nm in a one-pot hydrothermal synthesis. As a proof-of-concept study, we chose a standard amino acid L-lysine (Lys) and a nonstandard amino acid L-carnitine (LC), which have a permanent zwitterionic form, as well as their salt derivatives L-lysine acetate (LysAc) and L-carnitine L-tartrate (LCLT). The structural flexibility of the amino acids allowed their better incorporation into zeolite crystals, and their stability and solubility ensured easy removal after the hydrothermal synthesis by a simple washing step, totally eliminating the need for an energy-intensive calcination process. With this novel approach, we successfully synthesized highly mesoporous LTA zeolites (named as MLTA–X–Y, where X is the utilized amino acid and Y is the synthesis stage). The mesopore diameter peaked in the range of 15–20 nm, larger than the <10 nm mesopore diameter obtained from surfactant-based strategies for mesoporous LTA zeolites,[14,17,45–47] making them highly suitable for large biomolecule adsorption and thus, the loadings for catalase enzyme (CAT) were more than doubled for the current MLTA zeolites compared to conventional microporous LTA zeolites (CLTA). The low cost and high structural diversity of amino acids and their biocompatibility opens a door to the easy access of a variety of hierarchical zeolites, which have a number of industrially important applications such as adsorbents, ion exchangers, and catalysts.

2. Experimental

2.1. Materials

All reagents were of analytical grade and used as purchased without further purification. Sodium hydroxide and catalase were purchased from Sigma Aldrich, sodium aluminate from General Reagent, and Ludox (25% aqueous solution) from Qingdao Ocean Co., Ltd. L-carnitine was obtained from Energy Chemical, tartaric acid from Beijing Ouhe Technology, calcium chloride from J&K, and L-lysine, L-lysine acetate salt and *O*-acetyl-L-carnitine (AcLc) hydrochloride from Adamas-beta. Commercial LTA and FAU were purchased from Acros. Catalase assay kit was obtained from Beijing Solarbio Science & Technology Co., Ltd.

2.2. Synthesis of mesoporous LTA zeolites

Mesoporous LTA zeolites were synthesized using amino acids as mesopore generating agents. In an example synthesis for MLTA–LC, 12.54 ml of Ludox (25%) was dissolved in 20 ml of deionized water, followed by the addition of a clear solution containing 2.4 g of NaOH and 4.92 g of $NaAlO_2$ dissolved in 34 ml of deionized water, using a peristaltic pump. After stirring at room temperature for 3 h, the solution was heated to 80 °C, and then a solution containing 4.8 g of L-carnitine in 5 ml of deionized water was added in. The resulting gel underwent crystallization at 100 °C for 20 h under constant stirring. The pH of the synthesis solution was monitored using a pH electrode (Mettler Toledo FE20), which indicated alkaline reaction conditions with a pH between 13–14. The obtained powder was collected using a refrigerated centrifuge and dried at 60 °C for more than 12 h, and the sample was named as MLTA–LC-unwashed. The supernatant was also collected for characterization. Some MLTA–LC-unwashed samples were washed with deionized water until the pH of the supernatant solution was close to 7, and dried at 60 °C for more than 12 h, designated as MLTA–LC-washed. To investigate the effect of high temperature calcination, some MLTA–LC-washed samples were calcined at 600 °C for 2 h in a muffle furnace, which were named as MLTA–LC-calcined. The molar compositions of MLTA–LC/Lys and LTA-AcLC were $1Al_2O_3 : 2SiO_2 : 2Na_2O : 130H_2O : 1$ LC/Lys/AcLC respectively. For MLTA–LysAc, the composition was $1Al_2O_3 : 2SiO_2 : 2Na_2O : 130H_2O : 0.5$ LysAc, and for MLTA–LCLT, the composition was $1Al_2O_3 : 2SiO_2 : 2Na_2O : 130H_2O : 0.25$ LCLT.

Conventional LTA was synthesized using a procedure similar to that for MLTA except that no amino acid was added and crystallization was conducted at 100 °C for 3 h. Commercial LTA with particle sizes of 1.8–2.3 μm was purchased from Acros as a reference sample.

2.3. Calcium cation exchange experiment

The calcined MLTA materials were first cooled to room temperature, and then ion-exchanged with calcium cation by

mixing 500 mg of zeolite with a 5 ml solution of calcium chloride in a sealed tube at 80 °C for 6 h. The Ca^{2+} exchanged zeolite was centrifuged, and washed with deionized water. This procedure was repeated twice, and then the collected sample was dried at 60 °C for more than 12 h. These samples were named as MLTA–X–Ca^{2+}, where X is the utilized amino acid.

2.4. Catalase adsorption experiment

Fresh solutions of catalase were prepared by dissolving 50 mg of catalase in 10 ml of pH = 7.2 phosphate buffer saline (PBS) solution at 0 °C under an ultrasonic environment. 100 mg of a zeolite sample was added to the enzyme solution, and stirred at 4 °C by magnetic stirring at 600 rpm. 300 μl suspension samples were periodically taken from the reaction mixture during the encapsulation process for characterization. Supernatant was collected *via* centrifugation at 10 000 rpm using a microcentrifuge and measured using a NanoDrop 2000c (Thermo Scientific) for protein concentration measurements.

2.5. Catalase activity measurement

Fresh solutions of catalase were prepared by dissolving 20 mg of catalase in 4 ml of pH = 7.2 phosphate buffer saline (PBS) solution at 0 °C under an ultrasonic environment. 40 mg of a zeolite sample was added to the enzyme solution, and stirred at 4 °C by magnetic stirring at 600 rpm for 24 h. Solid with immobilized catalase was collected *via* centrifugation at 10 000 rpm using a microcentrifuge, and dispersed in a PBS buffer to a catalase concentration of 0.05 mg ml^{-1}. Catalase activity was measured using a catalase assay kit from Bejing Solarbio Science & Technology Co., Ltd (product #BC0760). Catalase was incubated at 37 °C for 2 h before examination of the activities, and all assays were performed at 37 °C. Catalase activity unit (U) was defined as the amount of 1 μmol of hydrogen peroxide decomposed by 1 milligram of catalase per second at 37 °C. The amount of degraded hydrogen peroxide was calculated by measuring the residual hydrogen peroxide concentration. The residual hydrogen peroxide was mixed with ammonium molybdate to form a complex with a maximum absorbance at a wavelength of 405 nm.

2.6. Characterization

Powder X-ray diffraction (XRD) patterns of zeolites were recorded using a Rigaku D/Max-2200 PC diffractometer in a diffraction angle range $2\theta = 4$–50° with Cu Ka radiation ($\lambda = 1.5418$ Å) at 40 kV, 40 mA. Scanning electron microscopy (SEM) was performed on a JEOL JSM-7800F electron microscope operated at 5.0 kV without coating the samples. Transmission electron microscopy (TEM) was performed on a Tecnai G2 F30 field emission source transmission electron microscope operated at 300 kV. The zeolite samples were ultramicrotomed to a thickness of 90 nm for TEM measurement after being embedded in Spurr's epoxy resin. Nitrogen adsorption–desorption isotherms were measured at −196 °C on a Micromeritics Tristar II 3020 v1.03 analyzer. The powder samples were degassed at 300 °C for at least 12 h before measurements. Brunauer–Emmett–Teller (BET) surface areas were calculated from the adsorption data from $0.05 < P/P_0 < 0.30$. Mesopore size distributions were determined using the Barrett–Joyner–Halenda (BJH) model. Micropore volumes were determined using a *t*-plot method. Si/Al ratios of the as synthesized samples were measured by inductively coupled plasma-atomic emission spectroscopy (ICP-AES, JY 2000-2). Centrifugation of suspension samples was conducted using a refrigerated centrifuge (Thermo Scientific Fiberlite F21s-8x50y). Thermogravimetric analyses (TGA) were performed on a Shimadzu TGA-50 analyzer. Fourier transform infrared spectroscopy (FTIR) spectra were recorded in KBr pellets using a Shimadzu IR-Prestige 21 Spectrophotometer. ^{1}H-NMR and ^{13}C-NMR measurements were performed using a 500 MHz nuclear magnetic resonance (NMR) spectrometer (Bruker nuclear resonance spectrometer). For solid samples, 300 mg of dry solid was dissolved in 10% hydrochloric acid solution or 5% hydrofluoric acid solution, followed by an evaporation and a drying step. The powders were dissolved into deuteroxide and filtered before a liquid NMR measurement. For liquid samples, 1 ml samples were dried and dehydrated, then dissolved into deuteroxide and filtered before a liquid NMR measurement. Protein concentrations were measured using a NanoDrop 2000c (Thermo Scientific). Absorbance values of the hydrogen peroxide–molybdate complexes were measured using a Shimadzu UV-2006 UV-Vis spectrophotometer.

3. Results and discussion

The powder X-ray patterns of the mesoporous LTA samples (Fig. 1) all exhibit peaks that can be indexed to a cubic unit cell of the LTA zeolite framework structure. Referenced to commercial NaA zeolites, similar peak intensities with crystallinities of *ca.* 96%, 94%, and 93% were obtained for CLTA, MLTA–LC-calcined, and MLTA–LCLT-calcined, respectively. The MLTA zeolites exhibit no obvious change of peak intensity and no distinct broadening of peak width, indicating the absence of nanocrystal aggregates, unlike surfactant mediated mesoporous LTA zeolites.[14,17,48] The structure of amino acid affected the crystal polymorph; while pure LTA was formed in the presence of

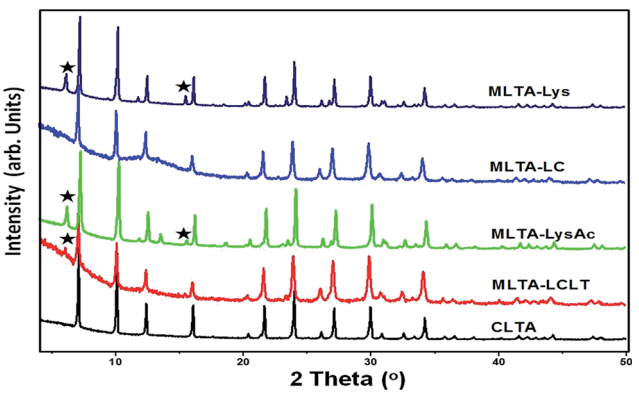

Fig. 1 Powder XRD patterns for mesoporous LTA zeolites synthesized with different amino acids and their derivatives: (a) Lys, (b) LC, (c) LysAc and (d) LCLT, in comparison with that of their conventional LTA counterpart (e). Diffraction peaks of FAU zeolite are marked with a ★. The powder samples were calcined at 600 °C for 2 h.

LC, other amino acids slightly induced FAU phase of less than 10%. The content of FAU phase in the LTA zeolite was calculated using a homogeneous mixture of 10% commercial FAU/90% commercial LTA purchased from Acros as a reference.

SEM images clearly reveal that all MLTA samples (Fig. 2a, b, S1a and b†) preserved a cubic-shaped crystal outline with truncated edges typical of crystalline LTA, with uniform particle sizes of about 1.1–1.4 μm. The micro-sized cubic particles are polycrystalline in nature, as clearly demonstrated in low-resolution TEM images (Fig. 2c and e), showing that the cubic-shaped MLTA particles are composed of elongated large crystallites with sizes of about 100 × 300 nm. On the contrary, a low resolution TEM image of conventional LTA samples (Fig. S1e†) indicates that CLTA particles in the SEM images are single crystals. Different from the smooth surfaces of microporous LTA (Fig. S1c and d†), MLTA samples exhibit obviously rugged surfaces indicating the distribution of mesopores within the particles. Mesopores with average pore sizes of about 22.0 ± 4.5 nm for MLTA–LC and 19.6 ± 4.7 nm for MLTA–LCLT were located within the LTA crystallites. These mesopores are disordered as illustrated by the high-resolution TEM images (Fig. 2d and f), which also show uniformly orientated lattice fringes over the entire image regions confirming the single crystalline nature of the MLTA zeolites. Therefore, the mesopores created with the amino acid 'porogens' are confined within LTA crystallites, which in turn constitute cubic-shaped MLTA particles oriented in similar growth directions as CLTA. The crystal topology of MLTA samples, the clearly patterned fast Fourier transform (FFT, insets of Fig. 2d and f) diffractograms, and the high XRD peak intensity, all demonstrate high crystallinity with no amorphous components.

The micropore structure analyses of conventional NaA zeolites are well known to be unattainable from N_2 adsorption isotherm measurement at 77 K because the micropore apertures in NaA zeolites are too narrow for N_2 molecules to diffuse rapidly in a reasonable equilibrium time.[17,49] As expected, almost no N_2 uptake was obtained for the conventional LTA samples. The mesoporous MLTA samples, on the other hand, all show a type IV N_2 adsorption isotherm with a steep step at P/P_0 in the range of 0.6–0.99 and an H_3 hysteresis loop without any limiting adsorption at high P/P_0 (Fig. 3a). This might be caused by capillary condensation of N_2 gas in the mesopores,[44,49] leading to an increased BET surface area, which is 90 and 104 $m^2\ g^{-1}$ for MLTA–LC and MLTA–LCLT respectively (Table 1). The mesopores (Fig. 3b) are between 10 to 50 nm in diameter, with a distribution peak centered at 15–20 nm, consistent with the observations from TEM images. The pores generated by amino acids are much larger than the 6–10 nm mesopores mediated by amphiphilic organosilane surfactants.[14] For the organosilane templated mesoporous LTA, an additional pore expansion agent such as EO–PO–EO triblock copolymer was needed to further expand the mesopore size beyond 10 nm.[17]

Noting that only noncovalent interactions were expected between amino acids and zeolite framework, it is interesting to find out the status of the amino acids in the as-synthesized MLTA zeolites and whether washing with water could remove these organic mesopore generating agents. Characterization techniques including TGA, FTIR, and NMR were performed on the unwashed and washed MLTA samples, and compared to

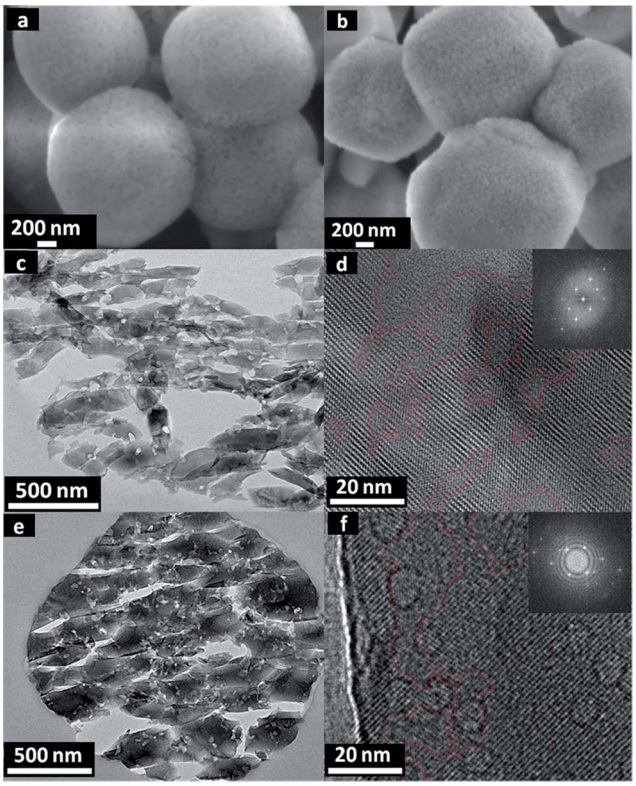

Fig. 2 SEM (a and b) and TEM (c–f) images of washed mesoporous LTA synthesized with different amino acids and their derivatives: (a) MLTA–LC, (b) MLTA–LCLT, (c) low-resolution TEM image, (d) HRTEM image of MLTA–LC, (e) low-resolution TEM image, and (f) HRTEM image of MLTA–LCLT; insets are the corresponding FFT diffractograms. Red marks are used in (d) and (f) as a visual guide to the intracrystalline mesopore areas in LTA crystallites.

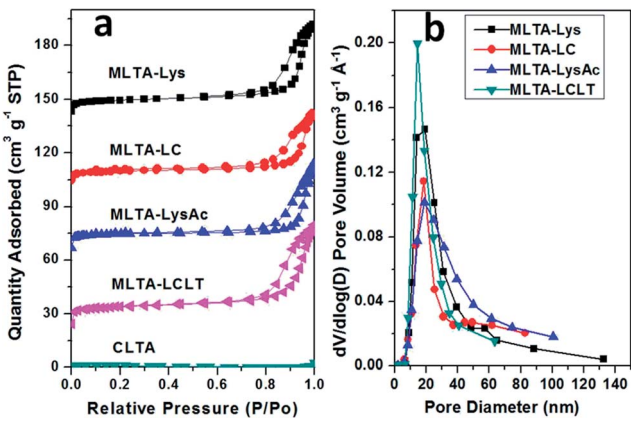

Fig. 3 (a) N_2 adsorption–desorption isotherms of washed mesoporous LTA zeolites synthesized with different amino acids and their derivatives in comparison with those of their conventional LTA counterparts. The isotherms for MLTA–Lys, MLTA–LC, MLTA–LysAc are vertically offset by 120, 80, 40 $cm^3\ g^{-1}$ respectively. (b) BJH mesopore size distribution corresponding to the desorption branch. All samples were degassed at 300 °C.

Table 1 Textural properties and catalase immobilization capacity of mesoporous LTA zeolites synthesized with various amino acids in comparison with those of conventional LTA samples

Sample	S_{BET}[a] ($m^2\ g^{-1}$)	d_{meso}[b] (nm)	V_{total}[c] ($cm^3\ g^{-1}$)	V_{meso}[d] ($cm^3\ g^{-1}$)	Si/Al[e]	CAT (mg g^{-1})	CAT activity[f] (U mg^{-1})	Relative activity[g] (%)
CLTA	N.O.[h]	N.O.	N.O.	N.O.	1.02	112	698.3	81.89
MLTA–LC	90	18.4	0.09	0.05	1.11	241	799.5	93.75
MLTA–LCLT	104	16.0	0.12	0.07	1.13	264	812.1	95.25
MLTA–Lys	89	19.1	0.11	0.07	1.16	179	815.7	95.66
MLTA–LysAc	141	19.0	0.12	0.07	1.14	208	768.7	90.15
CLTA–Ca^{2+}	476	<1.7	0.26	0.03	—	—	—	—
MLTA–LC–Ca^{2+}	492	18.3	0.30	0.07	—	—	—	—
MLTA–LCLT–Ca^{2+}	445	18.9	0.30	0.11	—	—	—	—
LTA–AcLC	1.5	N.O.	N.O.	N.O.	—	—	—	—

[a] S_{BET} is the BET surface area obtained from N_2 adsorption isotherm in a relative pressure range of 0.05–0.30. [b] Mesopore diameter calculated from the desorption branch using the BJH method. [c] Total pore volume calculated as the amount of N_2 adsorbed at $P/P_0 = 0.98$. [d] Mesopore volume calculated as (total pore volume – V_{mic} obtained from a *t*-plot method). [e] Si/Al ratios of the as synthesized samples were measured using inductively coupled plasma-atomic emission spectroscopy (ICP-AES). [f] CAT activity was calculated by U $mg^{-1} = (OD_{contrast} - OD_{sample}) \times 271/60/m_{CAT}$, CAT activity was measured after 24 hours. [g] Relative activity was compared to the pure catalase with a CAT activity of 852.7 U mg^{-1}. [h] N.O. data cannot be explicitly obtained. All samples were degassed at 300 °C for at least 12 h.

those performed on calcined samples, CLTA samples, and amino acid templates, which unambiguously proved the presence of amino acids in the as-synthesized MLTA samples and that water-washing could remove the amino acid templates completely. The TGA profiles (Fig. 4) of MLTA–LC-unwashed show a total weight loss of 29%, which is larger than the 19% observed for MLTA–LC-washed. The 10% weight loss difference could be attributed to the removal of residual L-carnitine template, which takes place at a temperature range between 200–550 °C, similar to the temperature range for free L-carnitine decomposition. The thermogravimetry profiles of MLTA–LC-washed, MLTA–LCLT-washed and CLTA samples are almost identical to each other with a difference of less than 5% (Fig. 4), and also to those of calcined samples (Fig. S2†), indicating a similar nature and amount of adsorbed species on all LTA samples, despite the mesoporosity. The onset weight loss temperature at ~60 °C and inflection point at ~160 °C observed for washed MLTA samples, also identifiable in the TGA curves of CLTA and calcined MLTA samples, are probably associated with the dehydration of physically adsorbed water, and the progressive dehydration of entrapped water.[44] These TGA profiles are markedly different from those for free LC whose onset weight loss began at 237 °C (Fig. 4), demonstrating a lack of amino acid in the MLTA samples.

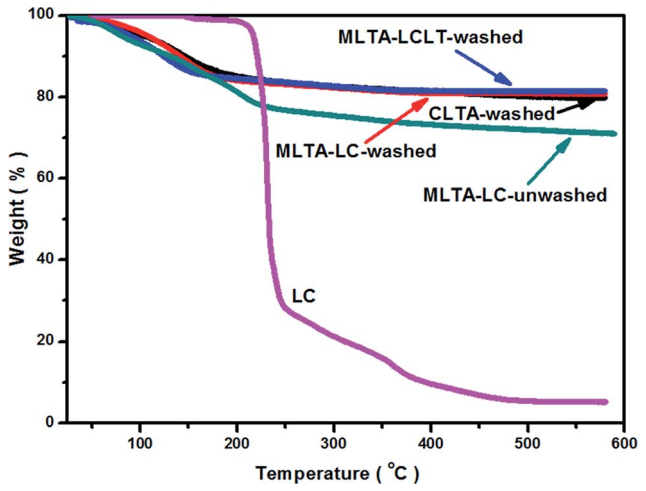

Fig. 4 Relative weight loss by TGA of as synthesized MLTA–LC and MLTA–LCLT samples after water washing in comparison with that of as synthesized CLTA, MLTA–LC-unwashed and free carnitine. All samples were degassed at 110 °C.

The FTIR spectra for MLTA–LC samples before and after calcination and the uncalcined CLTA sample (Fig. 5) all show distinctive absorption bands at around 465, 559, 667 and 1003 cm^{-1}, assigned to T–O (T = Si and Al) bending, external vibration of double rings (d4r), internal vibration of T–O symmetric, and asymmetric stretching,[50] respectively, in the LTA structure. The intense band at 1640 cm^{-1} can be ascribed to the bending mode of water molecules. Characteristic FTIR peaks of L-carnitine (Fig. 5) at 1582 and 1394 cm^{-1}, assigned to carboxylate groups, can be found in the spectrum of the MLTA–LC-unwashed sample, with a slight redshift to the wavenumbers of 1571 and 1379 cm^{-1}. Therefore, the amino acid LC not only remained in the as-synthesized MLTA sample, but also interacted with the zeolite framework. These peaks are absent in the spectra of the MLTA–LC-washed and MLTA–LC-calcined samples as well as the MLTA–LCLT-washed and MLTA–LCLT-calcined samples (Fig. S3†), thus it is dubious that any amino acid was still present in the water-washed samples. ^{13}C-NMR spectra of the unwashed MLTA–LC samples (Fig. S4b†) show all the characteristic peaks of the L-carnitine template, similar to that of the filtered synthesis solution (Fig. S4a†). For the water-washed MLTA–LC samples, neat ^{13}C-NMR exhibited no residual organic molecules (Fig. S5b†) and ^{1}H-NMR (Fig. S5a†) only showed a sharp peak of water. The complete disappearance of the L-carnitine peaks in the ^{13}C-NMR spectra after the as synthesized MLTA samples were washed with water proves the effectiveness of water-washing. Therefore, we can be sure that amino acid templates could be totally removed by a simple step of water washing, without the need for a calcination step. The

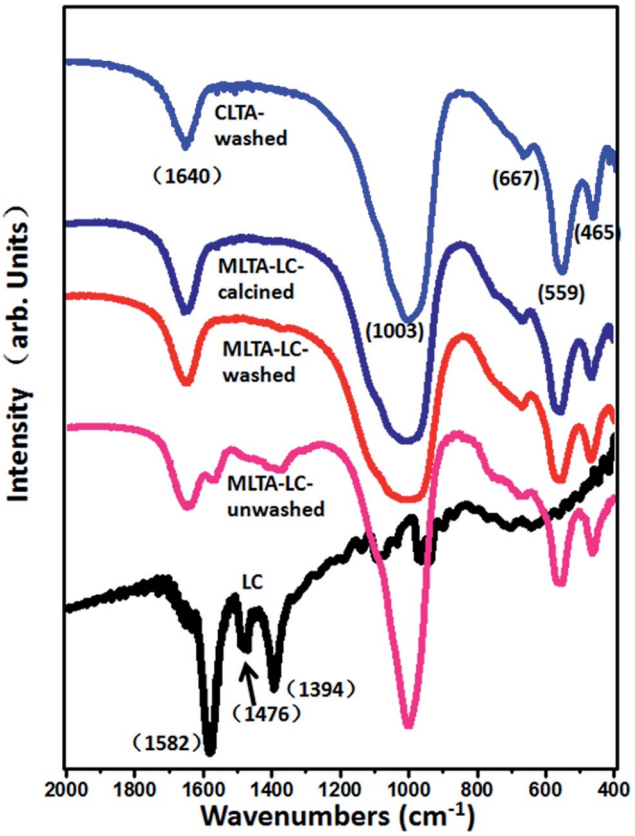

Fig. 5 FTIR spectra of the MLTA–LC sample as synthesized, after water-washing, and after calcination at 600 °C, in comparison with those of the as synthesized CLTA and free carnitine. All samples were degassed at 110 °C.

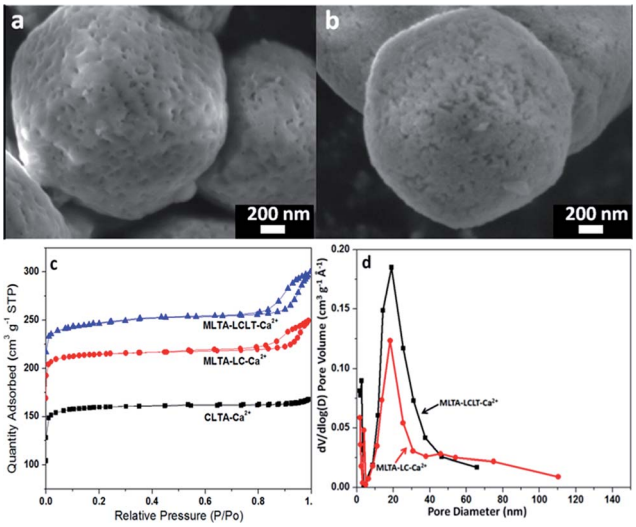

Fig. 6 Properties of calcined and Ca^{2+} exchanged mesoporous LTA samples: (a) SEM images of MLTA–LC–Ca^{2+}, (b) SEM images of MLTA–LCLT–Ca^{2+}, (c) N_2 adsorption–desorption isotherms; the isotherms for MLTA–LC–Ca^{2+} and MLTA–LCLT–Ca^{2+} are vertically offset by 50 and 100 $cm^3\ g^{-1}$, respectively, and (d) BJH mesopore size distribution corresponding to the desorption branch.

almost identical SEM images and pore structure analysis results obtained for MLTA–LC-washed and MLTA–LC-calcined samples further support this conclusion.

The mesopores were stable upon calcination and ion exchange. Both the crystal morphology (Fig. 6a and b) and the N_2 adsorption–desorption isotherms (Fig. 6c), as well as the mesopore size distribution (Fig. 6d) were almost unaltered. Calcium exchange increased the adsorbed amount of nitrogen and BET surface area (Table 1) as the Ca^{2+} cation is known to increase the α-cage aperture to 0.48 nm, enough for rapid uptake of N_2 molecules with a kinetic diameter of 0.44 nm into LTA zeolite framework micropores. Calcium exchange further confirmed the lack of mesopores in CLTA powders as the BJH pore size of CLTA–$Ca^{2+}$was less than 1.7 nm.

The quaternary ammonium group in the amino acids probably acts as a structure-directing agent for hierarchical zeolites, similar to the case of cationic polymer-based dual function templates, which strongly interact with the negatively charged aluminosilicate framework *via* Coulomb forces. On the other hand, the 15–20 nm average mesopore diameters are too large to be explained by the molecular size of the amino acids and their derivatives. Self-assembly of amino acids within the confined space of growing MLTA *via* strong hydrogen bonding was suspected to be the main reason, and thus the carnitine structural analogue *O*-acetyl-L-carnitine with the side chain hydroxyl group protected was used to elucidate the mesopore formation mechanism.

Shielding the hydrogen bonds of carnitine resulted in smooth cubic LTA crystals (Fig. 7) with a BET surface area of only 1.5 $m^2\ g^{-1}$ (Table 1) and no mesopores. Therefore, the hierarchical structure likely starts from cooperative assembly *via* electrostatic interactions between the negatively charged frameworks of pre-zeolitic units and the 3-dimensional network of amino acids linked by extensive hydrogen bonding (Scheme 1). The mesopore size range of 10–50 nm is in consensus with the prebiotic organic polymer system on mineral surfaces, having desired lengths in the range of 30–100 mers of amino acids.[51] Absence of covalent bonding with the zeolite framework and the high solubility of amino acids in water allowed their dissolution into the washing water.

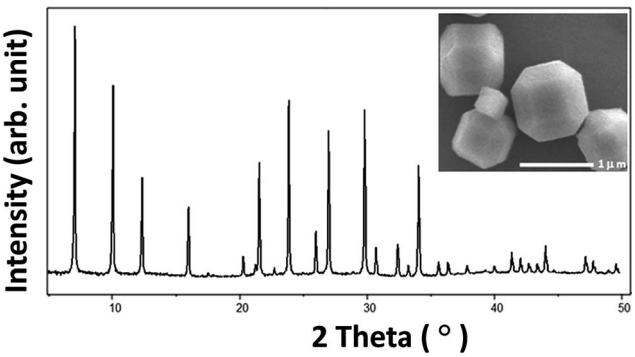

Fig. 7 Powder XRD pattern for LTA synthesized with *O*-acetyl-L-carnitine hydrochloride, the inset shows the SEM image. The powder samples were calcined at 600 °C for 2 h.

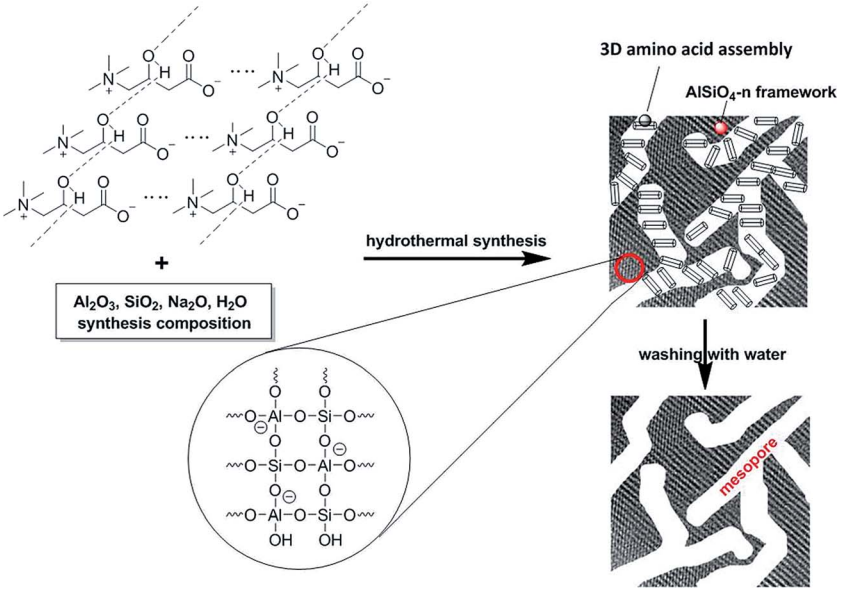

Scheme 1 Proposed mechanism for amino acid mediated mesoporous LTA formation.

The creation in a biologically compatible way of hierarchical structures containing >10 nm mesopores can remarkably benefit the immobilization and encapsulation of biomacromolecules, which could not enter the small micropores in conventional LTA. Therefore, the immobilization of relatively large enzymes was tested. The bovine liver catalase enzyme (hydrogen peroxide oxidoreductase EC 1.11.1.6) is a glycoprotein containing four polypeptide chains, each over 500 amino acids long, with a molecular size of ~10 nm, and is widely used in industry for catalyzing the degradation of hydrogen peroxide into water and oxygen. The mesoporous MLTA samples all exhibited a much higher catalase enzyme adsorption capacity (*e.g.*, 264 mg g^{-1} for MLTA–LCLT), more than double that of conventional LTA (Fig. 8). The adsorption kinetics were almost identical after the MLTA samples were calcined (Fig. S6†), again confirming that the enhanced adsorption was due to the mesopores created by the amino acid 'porogen' that could be fully removed by a simple washing step. As zeolite LTA with low Si/Al ratio is famous for its extreme hydrophilicity, such a high enzyme immobilization capacity is probably due to electrostatic interaction and hydrogen bonding. The absence of the hydrophobic effect could better protect the enzymes from denaturation induced by conformational change to expose their hydrophobic residues which are normally buried within the enzyme molecule.[52]

As a result, the catalase enzyme immobilized on all MLTA samples retained more than 90% of the enzymatic activity of the equivalent free catalase molecules (Table 1), much higher than the <20% reported for functionalized carbon nanotubes,[53] ~5% for graphite,[54] or <3% for the metal–organic framework ZIF-90.[52] This suggests that the hydrophilic MLTA mesopore surfaces induced almost no structural changes of catalase during the adsorption process. The conventional LTA exhibited 82% retained catalase enzyme activity, ~10% lower than the hierarchical MLTA samples, probably due to the mass transport

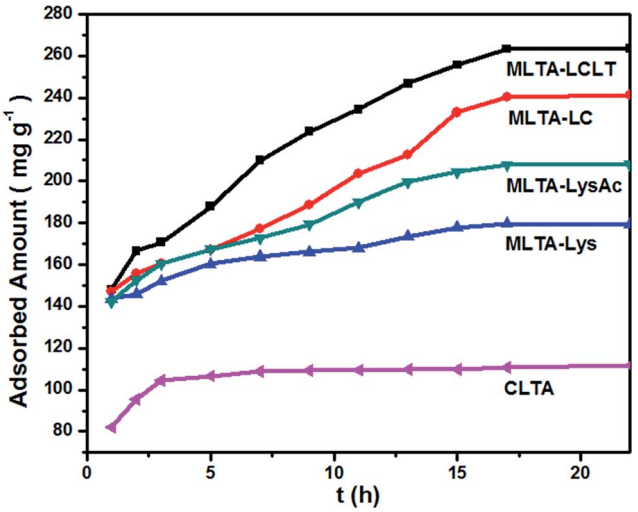

Fig. 8 Catalase adsorption kinetics on water-washed MLTA synthesized with different amino acids and CLTA. All samples were degassed at 110 °C.

limitations or the non-optimized interface between LTA and catalase. To demonstrate the storage stability of the immobilized enzyme, all samples were stored at 4 °C in a refrigerator for 15 days. Almost no decline in catalase activity was detected, especially for MLTA–LCLT with the highest catalase loading (Fig. S7†). The superiority of mesoporous LTA zeolites mediated by amino acids implies that this material can be used as a cheap and safe protein medicament carrier in the future.

4. Conclusions

In summary, we developed a new strategy for synthesizing mesoporous zeolite using amino acids as mesopore-generating agents. A variety of amino acids showed the ability to direct

mesopore formation in zeolite LTA. This novel approach exhibited several advantages including easy handling, being easy to scale up, and environmental friendliness. The mesoporous MLTA zeolite features a large surface area, large mesopores over 10 nm, higher adsorption capacity towards large biomolecules, and higher retained activity of an immobilized enzyme. The use of a non-surfactant and non-polymeric biomolecule template ensured high crystallinity of the zeolite framework and easy template removal by simple washing, substituting the energy-consuming calcination process. We believe that this novel synthesis strategy can be employed for a wide range of zeolite structures, opening a door to a new range of zeolitic materials. In addition to enzyme immobilization, the mesoporous zeolites produced in the present approach have great potential for other important applications such as heterogeneous catalysis, building segments for separation membranes, and drug delivery vehicles. Relevant studies on the synthesis mechanism as well as potential applications are currently underway.

Acknowledgements

We thank Dr Lianbing Ren and Dr Chao Teng for helpful discussion. Financial support was provided by the Guangdong Government (2013A061401002), Shenzhen Government (SGLH20131010153302024, JCYJ20140419131807792, CXZZ20140419131807788), and the Nanshan District of Shenzhen, China (FG2014JNYF0017A). Z. C. would like to thank the PKUSZ Dean's fund (2014013).

Notes and references

1 S. Lopez-Orozco, A. Inayat, A. Schwab, T. Selvam and W. Schwieger, *Adv. Mater.*, 2011, **23**, 2602–2615.
2 L.-H. Chen, X.-Y. Li, J. C. Rooke, Y.-H. Zhang, X.-Y. Yang, Y. Tang, F.-S. Xiao and B.-L. Su, *J. Mater. Chem.*, 2012, **22**, 17381.
3 D. P. Serrano, J. M. Escola and P. Pizarro, *Chem. Soc. Rev.*, 2013, **42**, 4004–4035.
4 K. Moller and T. Bein, *Chem. Soc. Rev.*, 2013, **42**, 3689–3707.
5 Y. Wei, T. E. Parmentier, K. P. de Jong and J. Zecevic, *Chem. Soc. Rev.*, 2015, **44**, 7234–7261.
6 L. Gueudre, M. Milina, S. Mitchell and J. Perez-Ramirez, *Adv. Funct. Mater.*, 2014, **24**, 209–219.
7 V. Valtchev, G. Majano, S. Mintova and J. Perez-Ramirez, *Chem. Soc. Rev.*, 2013, **42**, 263–290.
8 R. J. White, A. Fischer, C. Goebel and A. Thomas, *J. Am. Chem. Soc.*, 2014, **136**, 2715–2718.
9 K. Na, C. Jo, J. Kim, K. Cho, J. Jung, Y. Seo, R. J. Messinger, B. F. Chmelka and R. Ryoo, *Science*, 2011, **333**, 328–332.
10 D. D. Xu, Y. H. Ma, Z. F. Jing, L. Han, B. Singh, J. Feng, X. F. Shen, F. L. Cao, P. Oleynikov, H. Sun, O. Terasaki and S. N. Che, *Nat. Commun.*, 2014, **5**, 4262.
11 L. M. Huang, W. P. Guo, P. Deng, Z. Y. Xue and Q. Z. Li, *J. Phys. Chem. B*, 2000, **104**, 2817–2823.
12 S. C. Christiansen, D. Y. Zhao, M. T. Janicke, C. C. Landry, G. D. Stucky and B. F. Chmelka, *J. Am. Chem. Soc.*, 2001, **123**, 4519–4529.
13 H. Wang and T. J. Pinnavaia, *Angew. Chem., Int. Ed.*, 2006, **45**, 7603–7606.
14 M. Choi, H. S. Cho, R. Srivastava, C. Venkatesan, D. H. Choi and R. Ryoo, *Nat. Mater.*, 2006, **5**, 718–723.
15 M. Choi, R. Srivastava and R. Ryoo, *Chem. Commun.*, 2006, 4380–4382, DOI: 10.1039/b612265e.
16 R. Srivastava, M. Choi and R. Ryoo, *Chem. Commun.*, 2006, 4489–4491, DOI: 10.1039/b612116k.
17 K. Cho, H. S. Cho, L. C. de Menorval and R. Ryoo, *Chem. Mater.*, 2009, **21**, 5664–5673.
18 A. Inayat, I. Knoke, E. Spiecker and W. Schwieger, *Angew. Chem., Int. Ed.*, 2012, **51**, 1962–1965.
19 Y. Seo, S. Lee, C. Jo and R. Ryoo, *J. Am. Chem. Soc.*, 2013, **135**, 8806–8809.
20 F. S. Xiao, L. F. Wang, C. Y. Yin, K. F. Lin, Y. Di, J. X. Li, R. R. Xu, D. S. Su, R. Schlogl, T. Yokoi and T. Tatsumi, *Angew. Chem., Int. Ed.*, 2006, **45**, 3090–3093.
21 D. H. Park, S. S. Kim, H. Wang, T. J. Pinnavaia, M. C. Papapetrou, A. A. Lappas and K. S. Triantafyllidis, *Angew. Chem., Int. Ed.*, 2009, **48**, 7645–7648.
22 J. Zhu, Y. H. Zhu, L. K. Zhu, M. Rigutto, A. van der Made, C. G. Yang, S. X. Pan, L. Wang, L. F. Zhu, Y. Y. Jin, Q. Sun, Q. M. Wu, X. J. Meng, D. L. Zhang, Y. Han, J. X. Li, Y. Y. Chu, A. M. Zheng, S. L. Qiu, X. M. Zheng and F. S. Xiao, *J. Am. Chem. Soc.*, 2014, **136**, 2503–2510.
23 Y. Zhang, K. Zhu, X. Duan, X. Zhou and W. Yuan, *J. Mater. Chem. A*, 2014, **2**, 18666–18676.
24 H. Shiraga, W. Min, W. J. Vandusen, M. D. Clayman, D. Miner, C. H. Terrell, J. R. Sherbotie, J. W. Foreman, C. Przysiecki, E. G. Neilson and J. R. Hoyer, *Proc. Natl. Acad. Sci. U. S. A.*, 1992, **89**, 426–430.
25 S. Albeck, J. Aizenberg, L. Addadi and S. Weiner, *J. Am. Chem. Soc.*, 1993, **115**, 11691–11697.
26 G. Yang and L. J. Zhou, *Sci. Rep.*, 2014, **4**, 6594.
27 K. Stuckenschneider, J. Merz and G. Schembecker, *J. Phys. Chem. C*, 2014, **118**, 5810–5819.
28 M. Bouchoucha, F. Tielens, F. Gaslain, F. CostaTorro, S. Casale, A. Palcic, V. Valtchev, J. F. Lambert and M. Jaber, *J. Phys. Chem. C*, 2015, **119**, 8736–8747.
29 R. Watanabe, T. Yokoi and T. Tatsumi, *J. Colloid Interface Sci.*, 2011, **356**, 434–441.
30 Y. Q. Deng, S. F. Yin and C. T. Au, *Ind. Eng. Chem. Res.*, 2012, **51**, 9492–9499.
31 J. Dhainaut, T. J. Daou, N. Bats, B. Harbuzaru, G. Lapisardi, L. Rouleau and J. Patarin, *Microporous Mesoporous Mater.*, 2013, **170**, 346–351.
32 Y. Tao, H. Kanoh and K. Kaneko, *Langmuir*, 2005, **21**, 504–507.
33 H. Y. Chen, J. Wydra, X. Y. Zhang, P. S. Lee, Z. P. Wang, W. Fan and M. Tsapatsis, *J. Am. Chem. Soc.*, 2011, **133**, 12390–12393.
34 H. Greer, P. S. Wheatley, S. E. Ashbrook, R. E. Morris and W. Zhou, *J. Am. Chem. Soc.*, 2009, **131**, 17986–17992.

35 L. Han, J. Yao, D. Li, J. Ho, X. Zhang, C.-H. Kong, Z.-M. Zong, X.-Y. Wei and H. Wang, *J. Mater. Chem.*, 2008, **18**, 3337.
36 S. Tanaka, N. Nakatani, H. Okada and Y. Miyake, *Top. Catal.*, 2010, **53**, 224–230.
37 L. Bonaccorsi, P. Calandra, M. A. Kiselev, H. Amenitsch, E. Proverbio and D. Lombardo, *Langmuir*, 2013, **29**, 7079–7086.
38 M. Choi, D. H. Lee, K. Na, B. W. Yu and R. Ryoo, *Angew. Chem., Int. Ed.*, 2009, **48**, 3673–3676.
39 D. H. Lee, M. Choi, B. W. Yu, R. Ryoo, A. Taher, S. Hossain and M. J. Jin, *Adv. Synth. Catal.*, 2009, **351**, 2912–2920.
40 R. Valiullin, J. Kärger, K. Cho, M. Choi and R. Ryoo, *Microporous Mesoporous Mater.*, 2011, **142**, 236–244.
41 K. Cho, R. Ryoo, S. Asahina, C. Xiao, M. Klingstedt, A. Umemura, M. W. Anderson and O. Terasaki, *Solid State Sci.*, 2011, **13**, 750–756.
42 F. Yan Chao, M. Ying, L. Fu Xiang, L. Zhi Ping and X. Jian Wei, *J. Porous Mater.*, 2013, **20**, 465–471.
43 G. Q. Song, H. T. Liu, F. X. Li, Z. P. Lv and J. W. Xue, *J. Porous Mater.*, 2014, **21**, 1101–1111.
44 F. Hasan, R. Singh and P. A. Webley, *Microporous Mesoporous Mater.*, 2012, **160**, 75–84.
45 X. Zhaoteng, M. Jinghong, H. Wenming, B. Xiang, K. Yuhong, L. Jianhong and L. Ruifeng, *J. Mater. Chem.*, 2012, **22**, 2532–2538.
46 J. Kim, C. Jo, S. Lee and R. Ryoo, *J. Mater. Chem. A*, 2014, **2**, 11905–11912.
47 G. Rioland, S. Albrecht, L. Josien, L. Vidal and T. J. Daou, *New J. Chem.*, 2015, **39**, 2675–2681.
48 F. Hasan, R. Singh, G. Li, D. Zhao and P. A. Webley, *J. Colloid Interface Sci.*, 2012, **382**, 1–12.
49 K. S. W. Sing, D. H. Everett, R. A. W. Haul, L. Moscou, R. A. Pierotti, J. Rouquerol and T. Siemieniewska, *Pure Appl. Chem.*, 1985, **57**, 603–619.
50 E. H. Flanigen, H. Khatami and H. A. Szymanski, in *Molecular Sieve Zeolites-I, Advances in Chemistry*, ed. E. Flanigen, *et al.*, American Chemical Society, Washington, DC, 1974.
51 I. Parsons, M. R. Lee and J. V. Smith, *Proc. Natl. Acad. Sci. U. S. A.*, 1998, **95**, 15173–15176.
52 F. K. Shieh, S. C. Wang, C. I. Yen, C. C. Wu, S. Dutta, L. Y. Chou, J. V. Morabito, P. Hu, M. H. Hsu, K. C. W. Wu and C. K. Tsung, *J. Am. Chem. Soc.*, 2015, **137**, 4276–4279.
53 C. Zhang, S. Luo and W. Chen, *Talanta*, 2013, **113**, 142–147.
54 R. C. Sosa, R. F. Parton, P. E. Neys, O. Lardinois, P. A. Jacobs and P. G. Rouxhet, *J. Mol. Catal. A: Chem.*, 1996, **110**, 141–151.